PHYSICAL REVIEW D **94,** 115015 (2016)

Phenomenology of dark matter in chiral $U(1)_X$ dark sector

P. Ko[*]

School of Physics, KIAS, Seoul 02455, Korea and Quantum Universe Center, KIAS, Seoul 02455, Korea

Takaaki Nomura[†]

School of Physics, KIAS, Seoul 02455, Korea

(Received 17 August 2016; published 9 December 2016)

We consider dark matter physics in a model for the dark sector with extra dark $U(1)_X$ gauge symmetry. The dark sector is composed of exotic fermions that are charged under both dark $U(1)_X$ and the standard model $SU(3)_C \times U(1)_Y$ gauge groups, as well as standard model singlet complex scalars Φ and X with nonzero $U(1)_X$ charge. In this model, there are two dark matter candidates—a scalar and a fermion—both of which are stabilized by accidental Z_2 symmetry. Their thermal relic density, and direct and indirect detection constraints are discussed in detail and we search for the parameter space of the model accommodating dark matter observations. We also discuss constraints from diphoton resonance searches associated with the scalar field which breaks the dark $U(1)_X$, in a way consistent with dark matter physics. In addition, implications for collider physics are discussed, focusing on the production cross section of the scalar boson.

DOI: 10.1103/PhysRevD.94.115015

I. INTRODUCTION

The standard model (SM) of particle physics has been very successful in describing experimental data at both low and high energies. However, there are several remaining unsolved issues that require physics beyond the minimal SM. Among these outstanding issues is explaining the nature of dark matter (DM), whose existence is confirmed through astronomical and cosmological observations.

The existence of DM indicates a dark sector which is hidden from current experiments and observations. The nature of this dark sector is an open question. However, as the SM is described by local gauge symmetries, it is plausible that the dark sector is also ruled by SM and/or hidden gauge symmetries. In this sense, some particles in the dark sector can have charges of the SM gauge group which would induce interesting phenomena. For example, the dark sector in supersymmetric extensions of the SM with R-parity conservation is composed of supersymmetric partners of SM particles, and most of them carry nonzero SM gauge charges. Moreover, we expect that these new particles in the dark sector may play a crucial role in explaining some anomalies observed in experiments.

Using the LHC's 2015 experimental data, an excess of events in the diphoton channel around $m_{\gamma\gamma} \simeq 750$ GeV was announced by both the ATLAS and CMS collaborations [1–4] where the $\sim$5 fb cross section for the process $pp \to R \to \gamma\gamma$ was indicated, with R being a resonant state. To obtain the above cross section, R is expected to couple with exotic particles which have electric charge and/or color in order to enhance the gluon fusion production of R and its decay branching fraction into the diphoton mode. Motivated by the 750 GeV diphoton excess, the present authors proposed a model for a dark sector with extra $U(1)_X$ dark gauge symmetry which is spontaneously broken, giving a massive dark photon Z' decaying into SM fermions via kinetic mixing with SM gauge bosons [5]. Note that a number of authors have previously attempted to interpret this excess [5–31]. However, the new LHC data in 2016 disfavor the diphoton excess [32,33], where the upper limit of the cross section is 750 GeV as $\sigma(pp \to R \to \gamma\gamma) \leq 1.21$ fb in the narrow-width approximation [33] (taking into account a 1σ fluctuation).

Although originally motivated by the 750 GeV diphoton excess, we find that our model is an interesting realization of a dark sector with extra $U(1)_X$ dark gauge symmetry.[1] In this model, we introduce dark fermions [which are vector-like under $SU(3)_C \times U(1)_Y$ gauge symmetry, but chiral under $U(1)_X$] and $U(1)_X$ charged scalar fields Φ and X to break the U(1) symmetry and to make charged/colored dark fermions decay into SM fermions and DM X. Since the dark fermions are chiral, their masses are generated by the spontaneous $U(1)_X$ breaking due to the nonzero vacuum expectation value (VEV) of the $U(1)_X$ charged scalar field Φ, which is a singlet under SM. The signal of the diphoton resonance is induced by the scalar boson ϕ associated with Φ, where its gluon-fusion production and diphoton decay processes are induced through the dark fermion loop since the dark fermions couple to Φ and some of them carry color/electric charges. Remarkably, the Yukawa couplings

[*]pko@kias.re.kr
[†]nomura@kias.re.kr

[1]Some other models related to dark matter and extra $U(1)_X$ gauge symmetry were studied, e.g., in Refs. [34–47].

between Φ and dark fermions are related to the masses of dark fermions, which makes our model predictive. Moreover, an accidental Z_2 symmetry appears in our setup which provides natural stability for DM. In our previous paper, the diphoton excess was mainly analyzed with a limited parameter space, but the phenomenology of DM is also interesting and worthy of a detailed analysis. Thus, in this paper we carry out a detailed analysis of DM physics—including the relic density, and direct and indirect detection in the model—to explore the allowed parameter space. Furthermore, we also discuss compatibility with the current constraint from the diphoton resonance search and implications for collider physics.

The paper is organized as follows. In Sec. II we review our model and show the particle contents and their mass spectra after spontaneous gauge symmetry breaking. We study the DM physics (such as the relic density, and direct and indirect detection constraints) to find the allowed parameter region in Sec. III. In Sec. IV we discuss the constraint from the diphoton resonance search and implications for collider physics. We give a summary and discussion in Sec. V.

II. THE MODEL

In this section we recapitulate our dark sector model proposed in Ref. [5]. We consider a dark sector with $\mathrm{U}(1)_X$ dark gauge symmetry, new fermions carrying both SM $\mathrm{SU}(3)_C \times \mathrm{U}(1)_Y$ quantum numbers and $\mathrm{U}(1)_X$ charges, and SM singlet complex scalar fields as summarized in Table. I. The new fermions are vector-like under the SM gauge symmetry but chiral under $\mathrm{U}(1)_X$. The gauge anomalies from triangle loops are canceled due to the appropriate $\mathrm{U}(1)_X$ charge assignments. The Yukawa interactions and the scalar potential which contain the new fields are given by

$$\begin{aligned} L_{\mathrm{Yukawa}} &= y^E \bar{E}_L E_R \Phi + y^N \bar{N}_L N_R \Phi^\dagger + y^U \bar{U}_L U_R \Phi^\dagger \\ &\quad + y^D \bar{D}_L D_R \Phi + y^{Ee^i} \bar{E}_L e_R^i X + y^{Uu^i} \bar{U}_L u_R^i X^\dagger \\ &\quad + y^{Dd^i} \bar{D}_L d_R^i X + \mathrm{H.c.}, \end{aligned} \tag{1}$$

TABLE I. Contents of new fermions and scalar fields and their charge assignments under the gauge symmetry $\mathrm{SU}(3) \times \mathrm{SU}(2)_L \times \mathrm{U}(1)_Y \times \mathrm{U}(1)_X$. We consider three families of dark fermions.

	Fermions								Scalar	
	E_L	E_R	N_L	N_R	U_L	U_R	D_L	D_R	Φ	X
SU(3)	**1**	**1**	**1**	**1**	**3**	**3**	**3**	**3**	**1**	**1**
SU(2)	**1**	**1**	**1**	**1**	**1**	**1**	**1**	**1**	**1**	**1**
$U(1)_Y$	-1	-1	0	0	$\frac{2}{3}$	$\frac{2}{3}$	$-\frac{1}{3}$	$-\frac{1}{3}$	0	0
$U(1)_X$	a	$-b$	$-a$	b	$-a$	b	a	$-b$	$a+b$	a

$$\begin{aligned} V &= \mu^2 H^\dagger H + \lambda (H^\dagger H)^2 + \mu_\Phi^2 \Phi^\dagger \Phi + \mu_X^2 X^\dagger X \\ &\quad + \lambda_\Phi (\Phi^\dagger \Phi)^2 + \lambda_X (X^\dagger X)^2 + \lambda_{H\Phi} (H^\dagger H)(\Phi^\dagger \Phi) \\ &\quad + \lambda_{HX} (H^\dagger H)(X^\dagger X) + \lambda_{X\Phi} (X^\dagger X)(\Phi^\dagger \Phi), \end{aligned} \tag{2}$$

where H denotes the SM Higgs doublet field and the index i denotes the SM fermion generation. In this setup, there appears an accidental Z_2 symmetry

$$X \to -X, \qquad F_L \to -F_L, \qquad F_R \to -F_R$$

which is not broken after $\mathrm{U}(1)_X$ gauge symmetry breaking. As a result the lightest Z_2-odd particle becomes stable and it can be a DM candidate if it is neutral. Thus, the complex scalar X and the lightest neutral dark fermion N could be our DM candidates. Note that this model is similar to the usual minimal supersymmetric SM, except that the dark partners of the SM fermions are fermions rather than scalars, and the complex scalar X plays the role of the neutralino lightest supersymmetric particle.

The gauge symmetry is broken after H and Φ develop their nonzero VEVs:

$$H = \begin{pmatrix} G^+ \\ \frac{1}{\sqrt{2}}(v + h + iG^0) \end{pmatrix}, \quad \Phi = \frac{1}{\sqrt{2}}(v_\phi + \phi + iG_\phi), \tag{3}$$

where $G^\pm$, G^0, and G_S are Nambu-Goldstone bosons which are absorbed by $W^\pm$, Z, and Z', respectively. The VEVs of the scalar fields are approximately given by

$$v \simeq \sqrt{\frac{-\mu^2}{\lambda}}, \qquad v_\phi \simeq \sqrt{\frac{-\mu_\Phi^2}{\lambda_\Phi}}, \tag{4}$$

where we assumed that $\lambda_{H\Phi}$ is negligible so that the mixing between the SM Higgs boson h and ϕ is negligibly small to be consistent with the current Higgs data analysis [24,48,49]. With this assumption, the masses of h and ϕ are given by

$$m_h \simeq \sqrt{2\lambda} v, \qquad m_\phi \simeq \sqrt{2\lambda_\Phi} v_\phi, \tag{5}$$

where the mass formula for h is mostly the same as that for the SM Higgs. With the VEV of Φ the mass matrices of new fermions are given by

$$M_F = \frac{y^F}{\sqrt{2}} v_\phi, \tag{6}$$

where $F = U, D, E, N$, M_F denotes the mass of the new fermion F, and we have suppressed the family indices for simplicity.

We write the kinetic term for the gauge fields $\tilde{B}_\mu$ and $\tilde{X}_\mu$ [which are from $\mathrm{U}(1)_Y$ and $\mathrm{U}(1)_X$, respectively] including kinetic mixing:

$$\mathcal{L}_{\rm kin} = -\frac{1}{4}W^a_{\mu\nu}W^{a\mu\nu} - \frac{1}{4}(\tilde{B}_{\mu\nu}, \tilde{X}_{\mu\nu})\begin{pmatrix} 1 & s_\chi \\ s_\chi & 1 \end{pmatrix}\begin{pmatrix} \tilde{B}^{\mu\nu} \\ \tilde{Z}'^{\mu\nu} \end{pmatrix}, \tag{7}$$

where $s_\chi \equiv \sin\chi$. Then, we diagonalize the kinetic terms using the nonunitary transformation,

$$\begin{pmatrix} \tilde{B}_\mu \\ \tilde{X}_\mu \end{pmatrix} = \begin{pmatrix} 1 & -t_\chi \\ 0 & 1/t_\chi \end{pmatrix}\begin{pmatrix} B_\mu \\ X_\mu \end{pmatrix}, \tag{8}$$

where $t_\chi = \tan\chi$. After Φ and H develop nonzero VEVs, we obtain the approximate mass matrix for the neutral gauge field,

$$\frac{1}{8}\begin{pmatrix} \tilde{Z} \\ X \end{pmatrix}^T\begin{pmatrix} (g^2+g'^2)v^2 & t_\chi g'\sqrt{g^2+g'^2}v^2 \\ t_\chi g'\sqrt{g^2+g'^2}v^2 & 4(a+b)^2 g_X^2 v_\phi^2 \end{pmatrix}\begin{pmatrix} \tilde{Z} \\ X \end{pmatrix}, \tag{9}$$

where we used $W^3_\mu = \cos\theta_W Z_\mu + \sin\theta_W A_\mu$ and $B_\mu = -\sin\theta_W Z_\mu + \cos\theta_W A_\mu$. In our analysis, we assume $\chi \ll 1$; actually, the kinetic mixing parameter is experimentally limited as roughly $\chi \lesssim 10^{-2}$–10^{-3} for $m_{Z'} \simeq O(100)$ GeV [50–52]. With this assumption, the neutral gauge boson masses are approximated by

$$m_Z^2 \simeq \frac{1}{4}(g^2+g'^2)v^2, \qquad m_{Z'}^2 \simeq (a+b)^2 g_X^2 v_\phi^2. \tag{10}$$

The mass eigenstates are also obtained as

$$\begin{pmatrix} Z_\mu \\ Z'_\mu \end{pmatrix} = \begin{pmatrix} \cos\theta & -\sin\theta \\ \sin\theta & \cos\theta \end{pmatrix}\begin{pmatrix} \tilde{Z}_\mu \\ X_\mu \end{pmatrix}, \tag{11}$$

and the $Z - Z'$ mixing angle is given by

$$\tan 2\theta \simeq \frac{g'\sqrt{g^2+g'^2}v^2}{2(m_Z^2 - m_{Z'}^2)}t_\chi, \tag{12}$$

which is suppressed by t_χ. Notice that Z' decays into the SM particles via the kinetic mixing so that $\Gamma(Z')/m_{Z'} \sim O(\chi^2) \lesssim 10^{-4}$. Therefore, Z' would be a very narrow resonance.

After $\mathrm{U}(1)_X$ symmetry breaking, the interactions of the physical scalar ϕ and h are obtained from the Yukawa coupling and scalar potential such that

$$\mathcal{L}_{\rm Yukawa} = \frac{y^E}{\sqrt{2}}\bar{E}_L E_R\phi + \frac{y^N}{\sqrt{2}}\bar{N}_L N_R\phi + \frac{y^U}{\sqrt{2}}\bar{U}_L U_R\phi + \frac{y^D}{\sqrt{2}}\bar{D}_L D_R\phi \tag{13}$$

$$V \supset \frac{1}{4}\lambda_{H\Phi}(hh)(\phi\phi) + \frac{1}{2}\lambda_{H\Phi}vh(\phi\phi) + \frac{1}{2}\lambda_{H\Phi}v_\phi\phi(hh) + \frac{1}{2}\lambda_{HX}(hh)(X^\dagger X) + \lambda_{HX}vh(X^\dagger X) + \frac{1}{2}\lambda_{X\Phi}(X^\dagger X)(\phi\phi) + \lambda_{X\Phi}v_\phi\phi(X^\dagger X). \tag{14}$$

Also, the gauge interaction of ϕ is given by

$$\mathcal{L} \supset g_X^2(a+b)^2 v_\phi\phi Z'^\mu Z'_\mu + \frac{1}{2}g_X^2(a+b)^2\phi\phi Z'^\mu Z'_\mu, \tag{15}$$

where we took $\cos\theta \simeq 1$ since $\theta \ll 1$ as indicated above. In the following analysis we just apply $\theta = 0$. The gauge interactions of DM candidates are given by

$$\mathcal{L} \supset -iag_X(\partial_\mu X^\dagger X - \partial_\mu X X^\dagger)Z'^\mu + a^2 g_X^2 Z'_\mu Z'^\mu X^\dagger X + g_X(a\bar{N}_L\gamma^\mu N_L - b\bar{N}_R\gamma^\mu N_R)Z'_\mu. \tag{16}$$

The gluon-gluon-ϕ coupling is induced by the new fermion loop, which is obtained as [53]

$$\mathcal{L}_{\phi gg} = \frac{\alpha_s}{8\pi}\left(\sum_{F=U,D}\frac{(a+b)\sqrt{2}g_X}{m_{Z'}}A_{1/2}(\tau_F)\right)\phi G^{a\mu\nu}G^a_{\mu\nu}, \tag{17}$$

where $A_{1/2}(\tau) = 2\tau[1 + (1-\tau)f(\tau)]$ with $f(\tau) = [\sin^{-1}(1/\sqrt{\tau})]$ for $\tau \geq 1$ and $\tau_F \equiv 4m_F^2/m_\phi^2$. Applying the relevant interactions, we can derive decay widths of ϕ into various channels, which are summarized in the Appendix.

III. DARK MATTER PHENOMENOLOGY

In this section, we discuss the phenomenology of dark matter in our model. The dark matter of our model is the lightest neutral particle which is odd under accidental Z_2 symmetry: the candidates are X and N. In this work we consider two schemes:

$$1): m_{\rm DM} < m_{Z'},$$
$$2): m_{\rm DM} > m_{Z'}.$$

Then, we focus on the processes DM $\overline{\rm DM} \to$ gluons and DM $\overline{\rm DM} \to Z'Z'$ as the dominant DM annihilation processes for schemes 1) and 2), respectively. Notice that the annihilation processes DM $\overline{\rm DM} \to f_{\rm SM}\overline{f_{\rm SM}}$ are also possible via $\bar{F}fX$ Yukawa interactions described by Eq. (2).

These interactions were already analyzed in Refs. [54,55] and we assume the contribution from the Yukawa contraction is small in our following analysis.

A. Relic density

Here we estimate the relic density of DM for both schemes 1) and 2) and search for the allowed parameter region of the model. To reduce the number of parameters in the analysis, we first fix some parameters in the model as follows:

$$M_E = 600\ \text{GeV}, \qquad M_U = M_D = 800\ \text{GeV},$$
$$m_\phi = 750\ \text{GeV}, \qquad \lambda_{HX} = 0, \qquad a \simeq 1, \qquad b \simeq 1, \tag{18}$$

where we assumed a vanishing Higgs portal coupling[2] and $a \neq b$. Then, we assume $m_{\rm DM} < M_{E,U,D}$ to stabilize DM. In the following, we shall set the mass of ϕ to be 750 GeV since this mass point is well investigated due to the 750 GeV diphoton resonance, and we will discuss the constraints from recent data on the diphoton resonance search in Sec. IV. We note that the phenomenology would not change much qualitatively when we change the value of m_ϕ, while some quantitative differences may appear for those processes where ϕ propagates in the s channel; the position of the resonant region changes as $m_{\rm DM} \simeq m_\phi/2$ and the required values of the coupling constants that could explain the thermal relic density of DM will get larger (smaller) for heavier (lighter) ϕ.

For scheme 1), the dominant DM annihilation processes are $X\bar{X}(N\bar{N}) \to \phi \to gg$ through the effective interaction (17), which is a good approximation as long as $m_{\rm DM} < m_F$. The DM annihilation cross section can be obtained in the nonrelativistic approximation:

$$(\sigma v_{\rm rel})_{XX\to gg} \simeq \left(\frac{m_{Z'}}{(a+b)g_X}\right)^2 \frac{\lambda_{X\Phi}^2}{(s-m_\phi^2)^2+\Gamma_\phi^2 m_\phi^2} \times \frac{\Gamma(\phi\to gg)_{m_\phi=2m_{\rm DM}}}{2m_{\rm DM}}, \tag{19}$$

$$(\sigma v_{\rm rel})_{NN\to gg} \simeq 2v_{\rm rel}^2 \frac{M_N^4}{m_{Z'}^2} \frac{(a+b)^2 g_X^2}{(s-m_\phi^2)^2+\Gamma_\phi^2 m_\phi^2} \times \frac{\Gamma(\phi\to gg)_{m_\phi=2m_{\rm DM}}}{2m_{\rm DM}}, \tag{20}$$

where s is the total center-of-mass energy, Γ_ϕ is the total width of ϕ, $\Gamma(\phi\to gg)_{m_\phi=2m_{\rm DM}}$ is the width for the $\phi\to gg$ decay with $m_\phi = 2m_{\rm DM}$, and we have used $v_\phi \simeq m_{Z'}/((a+b)g_X)$. We note that $N\bar{N}\to gg$ does not have a contribution from the S wave, and the P-wave contribution is dominant. For $X\bar{X}\to gg$, the annihilation cross section is almost independent of g_X and $m_{Z'}$ except for the resonant region around $m_X \sim m_\phi/2$ when we apply Eq. (A1) to Eq. (19). We thus scan g_X in the region $\{0.1, 1.0\}$ and fix $m_{Z'} = 500$ GeV for simplicity. On the other hand, the annihilation cross section depends on g_X and $m_{Z'}$ for the $N\bar{N}\to gg$ process. Note that we fix $\lambda_{X\Phi} = 0$ for the fermion DM case since $\lambda_{X\Phi}$ is an irrelevant parameter in this case. In this scheme, the total decay width of ϕ can be approximated as $\Gamma_\phi \simeq \Gamma(\phi\to gg) + \Gamma(\phi\to XX)$ since other modes are sufficiently small. The relic density of DM is then obtained by solving the Boltzmann equation. The approximated formula for the relic density is also given by [56]

$$\Omega h^2 \approx \frac{1.07\times 10^9\ [\text{GeV}]^{-1}}{g_*^{1/2} M_{\rm pl} \int_{x_f}^\infty \frac{dx}{x^2} \langle\sigma v_{\rm rel}\rangle_{\rm anni}}, \tag{21}$$

where $\langle\sigma v_{\rm rel}\rangle_{\rm anni}$ is the thermal average of $\sigma v_{\rm rel}$ which is a function of $x \equiv m_{\rm DM}/T$ with temperature T, x_f is x at the freeze-out temperature, g_* is the total number of effective relativistic degrees of freedom at the time of freeze-out, and $M_{\rm pl} = 1.22\times 10^{19}$ [GeV] is the Planck mass. To estimate the relic density, we use micrOMEGAs 4.1.5 [57] where the Boltzmann equation is numerically solved by implementing relevant interactions for the annihilation processes. Then, in our numerical analysis below, we set the approximated allowed region for the relic density to be [58]

$$0.11 \lesssim \Omega h^2 \lesssim 0.13. \tag{22}$$

In Fig. 1, we show the parameter region which can account for the DM thermal relic density for scalar and fermion DM cases in the left and right plots, respectively. For the scalar DM case, we find that the required value of $\lambda_{X\Phi}$ becomes small at $m_X \sim m_\phi/2$ due to the resonant enhancement of the annihilation cross section. For the fermion DM case, the dependence of g_X on $m_{Z'}$ is not trivial and we show cases of $m_{Z'} = 1.1(2.0)m_N$ in the right plot of Fig. 1.

Here we comment on the case with a non-negligible $h-\phi$ mixing $\alpha \sim O(0.1)$. In this case, the DM annihilation processes $XX(NN)\to\phi\to W^+W^-/ZZ$ can be sizable via the scalar mixing effect if $m_{X(N)} \gtrsim O(100)$ GeV. Thus the parameter region satisfying the thermal relic density of DM would change for scalar DM with $\lambda_{X\Phi}\neq 0$ and for fermion DM. In particular, significant changes would appear for the parameter region for scheme 1) due to a small coupling of the ϕgg interaction [see Eq. (17)].

For scheme 2), we also numerically estimate the thermal relic density of DM using micrOMEGA s 4.1.5to solve the Boltzmann equation by implementing relevant interactions

[2]The Higgs portal interaction would have little effect our analysis as long as $\lambda_{XH} \lesssim 0.1$, since the DM annihilation cross section becomes less than 1/10 of the cross section to provide the observed relic density. Therefore, we shall take $\lambda_{XH} = 0$ hereafter for simplicity.

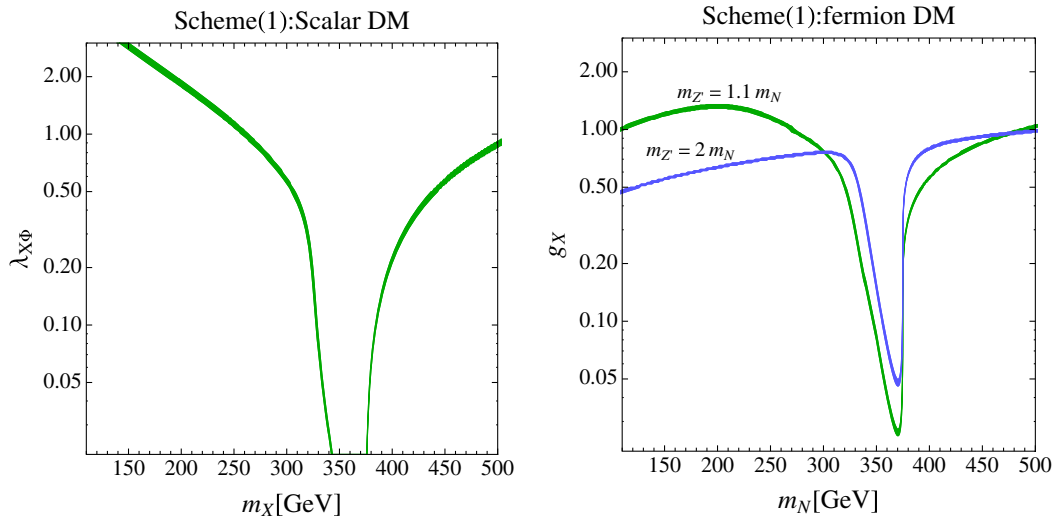

FIG. 1. The parameter region explaining the observed relic density of DM in the m_X-$\lambda_{X\Phi}$ and M_N-g_X planes for scalar and fermionic DM cases, respectively, in scheme 1).

which induce (co)annihilation processes of DM, $X\bar{X}(N\bar{N}) \to Z'Z'$. The annihilation processes $X^*X(\bar{N}N) \to Z'Z'$ are induced via the gauge interaction (16) and ϕ exchange in the s channel. Thus, the coupling constants g_X and $\lambda_{X\Phi}$ and the DM masses are relevant parameters in estimating the relic density of the DM. We also run the Z' mass in the range of $0.3 \times m_X \leq m_{Z'} \leq 0.9 \times m_X$ to make the process kinematically allowed. The left plot in Fig. 2 shows the parameter region which explains the relic density of the scalar DM in the g_X-m_X plane where we take $\lambda_{X\Phi} = 0$ and $M_N = 600$ GeV. In this case, we find that a ∼0.15 to ∼0.45 gauge coupling can provide the observed relic density when the DM mass is ∼100 to ∼500 GeV. On the other hand, the right plot Fig. 2 shows the parameter region in the $\lambda_{X\Phi}$-m_X plane where we take $g_X = 0.1$, 0.2, and 0.3 as reference values. We notice that $\lambda_{X\Phi}$ should be very small for $m_X \sim m_\Phi/2$ since the annihilation cross section gets the Breit-Wigner enhancement. For the case of fermion DM, we show the parameter region explaining the correct thermal relic density of DM in the g_X-M_N plane in Fig. 3. We find that the s-channel process $N\bar{N} \to \phi \to Z'Z'$ provides the dominant contribution to the annihilation cross section for $M_N \sim m_{Z'}/2$.

B. Direct detection

In our model, DM-nucleon scattering occurs through the processes exchanging h, ϕ, and Z' bosons. The Z' exchange will provide a small amplitude since it involves Z-Z' mixing which can be sufficiently small. Similarly, the Higgs exchange contribution can be made small enough if we take a small λ_{HX}. Therefore, we shall focus on the ϕ

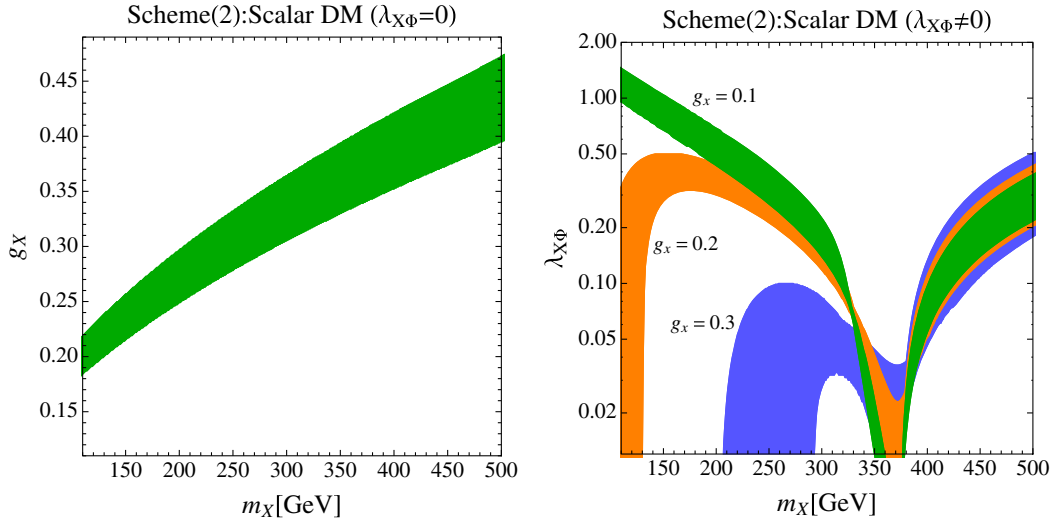

FIG. 2. The left (right) plot shows the parameter region explaining the observed relic density of DM in the g_X-m_X ($\lambda_{X\Phi}$-m_X) plane for scalar DM in scheme 2).

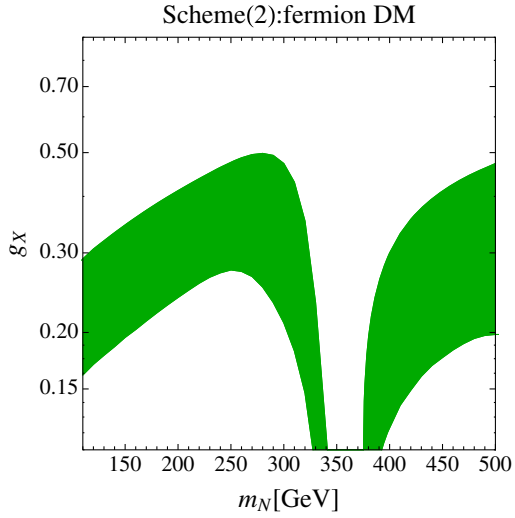

FIG. 3. The parameter region explaining the observed relic density of DM in the g_X-M_N plane for fermion DM in scheme 2).

exchange, which provides a contribution to DM-nucleon scattering amplitude from ϕ-gluon-gluon coupling in Eq. (17) and $\phi XX(\phi NN)$ coupling even if we ignore the ϕ-h mixing. The effective couplings for $XX(NN)$-gg can be estimated as

$$\mathcal{L}_{XXGG} = \frac{\alpha_S}{4\pi}\left(\sum_{F=U,D}\frac{\lambda_{X\Phi}}{m_\phi^2}A_{1/2}(\tau_F)\right)X^\dagger X G^{a\mu\nu}G^a_{\mu\nu} \equiv \frac{\alpha_S}{4\pi}C_g^X X^\dagger X G^{a\mu\nu}G^a_{\mu\nu}, \quad (23)$$

$$\mathcal{L}_{NNGG} = \frac{\alpha_S}{4\pi}\left(\sum_{F=U,D}\frac{2\sqrt{2}g_X^2 M_N}{m_\phi^2 m_{Z'}^2}A_{1/2}(\tau_F)\right)\bar{N}NG^{a\mu\nu}G^a_{\mu\nu} \equiv \frac{\alpha_S}{4\pi}C_g^N \bar{N}NG^{a\mu\nu}G^a_{\mu\nu}. \quad (24)$$

The spin-independent $X(N)$-nucleon scattering cross section is obtained as [55]

$$\sigma^X_{\rm SI} = \frac{m_{Nu}^2}{\pi(m_X+m_{Nu})^2}(f^X_{Nu})^2, \quad (25)$$

$$\sigma^N_{\rm SI} = \frac{2m_N^2 m_{Nu}^2}{\pi(m_N+m_{Nu})^2}(f^N_{Nu})^2, \quad (26)$$

$$\frac{f^{X(N)}_{Nu}}{m_{Nu}} = -\frac{2}{9}C_g f^{(Nu)}_{T_G}, \quad (27)$$

where m_{Nu} is the nucleon mass and $f^{(Nu)}_{T_G}$ is the mass fraction of gluonic operators in the nucleon mass. For the numerical values for these parameters, we adopt the values in Ref. [59]. In Figs. 4 and 5 we show the spin-independent DM-nucleon scattering cross section where the allowed parameter regions from the relic density estimation are applied. In scheme 1), we find that the parameter region with $m_X \lesssim 200$ GeV is excluded for scalar DM and $m_N \lesssim 300$ GeV is excluded for fermion DM with $m_{Z'} = 1.1 m_N$, by the current constraints of the LUX experiment [60,61]. Except for the resonant region, most of the parameter region can be tested in future direct detection experiments such as XENON 1t [62]. In scheme 2), we find that only the parameter region with small g_X and $m_X \lesssim 150$ GeV is constrained by the LUX data. The other region will be explored by future experiments.

C. Indirect detection

Here we discuss indirect detection of DM. In our model, DM pairs annihilate dominantly into gg and $Z'Z'$ in schemes 1) and 2), respectively, and Z' will further decay into SM fermions via kinetic mixing.

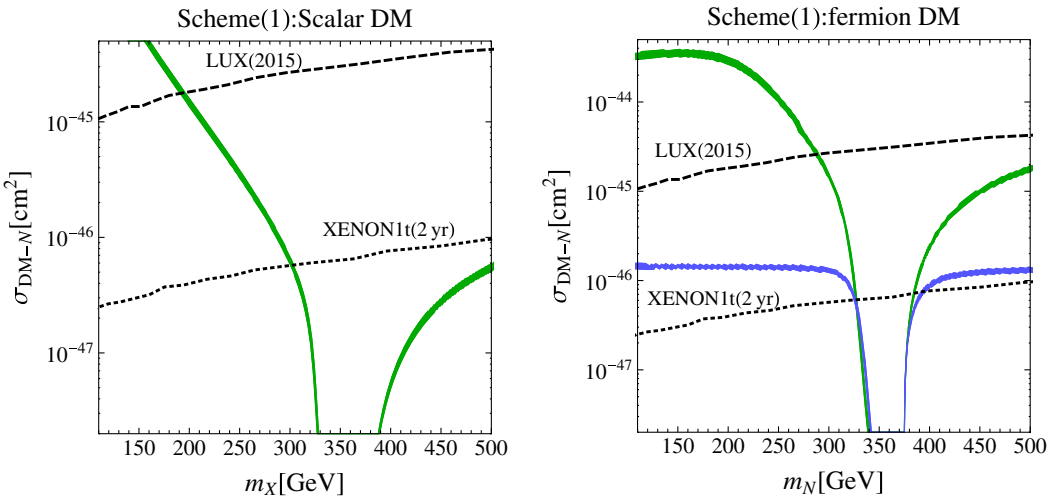

FIG. 4. The DM-nucleon scattering cross section as a function of DM mass for scheme 1) where the parameters satisfying the observed relic density in Fig. 1 are applied. The left and right plots correspond to scalar and fermionic DM cases, respectively.

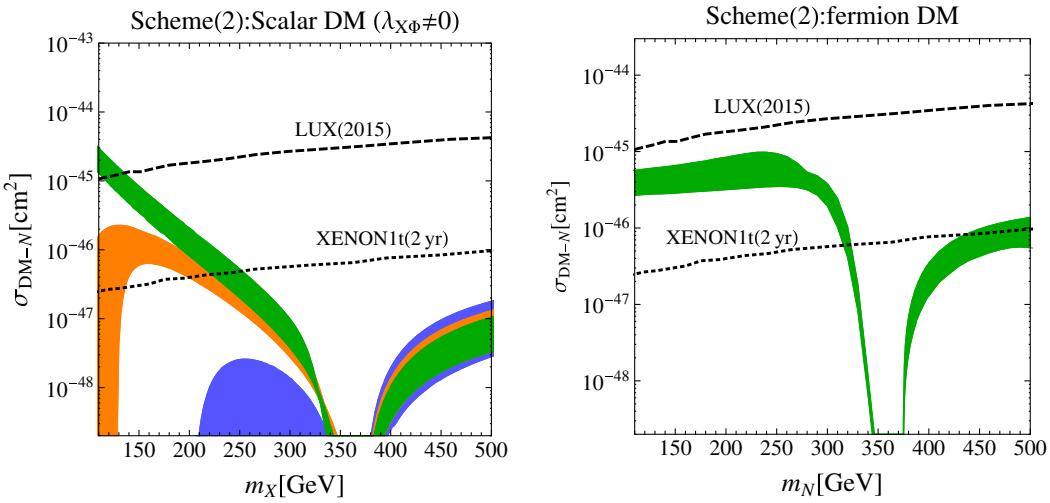

FIG. 5. The DM-nucleon scattering cross section as a function of DM mass for scheme 2) where the parameters satisfying the observed relic density in Figs. 2 and 3 are applied.

For scheme 1) the present-day annihilation cross sections for $XX(NN) \to gg$ are estimated using micrOMEGAs 4.1.5 where parameter sets providing the observed relic density are applied as inputs. In the case of scalar DM, we obtain the thermally averaged cross section $\langle\sigma v\rangle_{XX\to gg}$ shown in Fig. 6 where the colored region corresponds to the parameter space in the left plot of Fig. 1. Here we compare the cross section with the current limit of the cross section for $DMDM \to b\bar{b}$ from Fermi-LAT [63], where the limit for the gg mode is indicated to be slightly weaker than the $b\bar{b}$ mode [27]. Thus the parameter region $m_X \simeq m_\phi/2$ is excluded due to resonant enhancement, while other regions are allowed. In the case of fermion DM, we find that the current thermally averaged annihilation cross section is much smaller than the constraint by Fermi-LAT since the $N\bar{N} \to \phi \to gg$ process is a t-channel one. Therefore, here we omit the plot for the cross section for fermion DM.

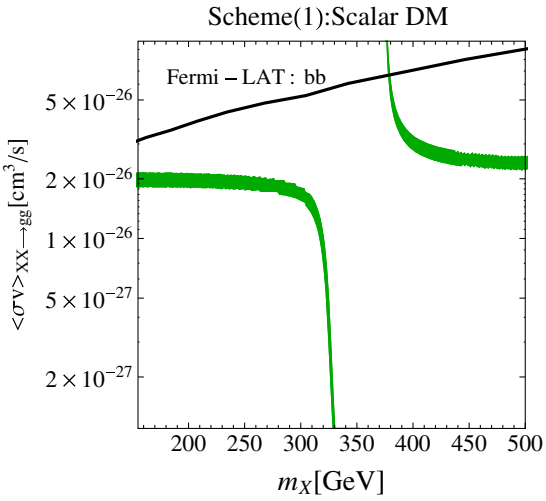

FIG. 6. The present-day thermally averaged cross section for $XX \to gg$ where the parameter region in Fig. 1 is applied. The black solid line indicates the current limit of the cross section for the DMDM $\to b\bar{b}$ annihilation mode from Fermi-LAT.

For scheme 2) we calculate the present-day thermally averaged DM annihilation cross sections $\langle\sigma v\rangle$ using micrOMEGAs 4.1.5 where we apply the parameters that are consistent with the relic density of DM. In this scheme the DM pair annihilate dominantly into a Z' pair, which provides four SM fermions in final states. To discuss constraints from indirect detection experiments, we consider the following effective cross section:

$$\langle\sigma v\rangle_{\mathrm{eff}} = \langle\sigma v\rangle_{\mathrm{DMDM}\to Z'Z'}[2\mathrm{BR}(Z'Z' \to 4f^C_{\mathrm{SM}}) + \mathrm{BR}(Z'Z' \to 2f^C_{\mathrm{SM}}2f^N_{\mathrm{SM}})], \quad (28)$$

where $\mathrm{BR}(Z'Z' \to 4f^C_{\mathrm{SM}})$ and $\mathrm{BR}(Z'Z' \to 2f^C_{\mathrm{SM}}2f^N_{\mathrm{SM}})$ are the branching fractions for both Z''s decaying into charged SM particles, and one Z' decaying into charged SM particles and the other Z' decaying into neutrinos, respectively, and the factor of 2 corresponds to the doubly charged flux from Z' decay. Figure 7 shows $\langle\sigma v\rangle_{\mathrm{eff}}$ for the parameter region in Fig. 2 which is compared with the constraints from Fermi-LAT for the DMDM $\to b\bar{b}(\tau\bar{\tau})$ annihilation mode [63]; the constraints from light quark modes are similar to the $b\bar{b}$ mode, while those from electron and muon pair modes are weaker than the tau pair mode. We note that our cross section cannot be directly compared with the constraints from the single annihilation mode since our Z' decays to all SM fermions. Notice also that we compare the effective cross section at m_X with experimental limits at $m_X/2$ since our final states have four particles and one particle carries an energy of $m_X/2$. Conservatively, we can say that the region $m_X \lesssim 200$ GeV is disfavored. As in scheme 1), the current

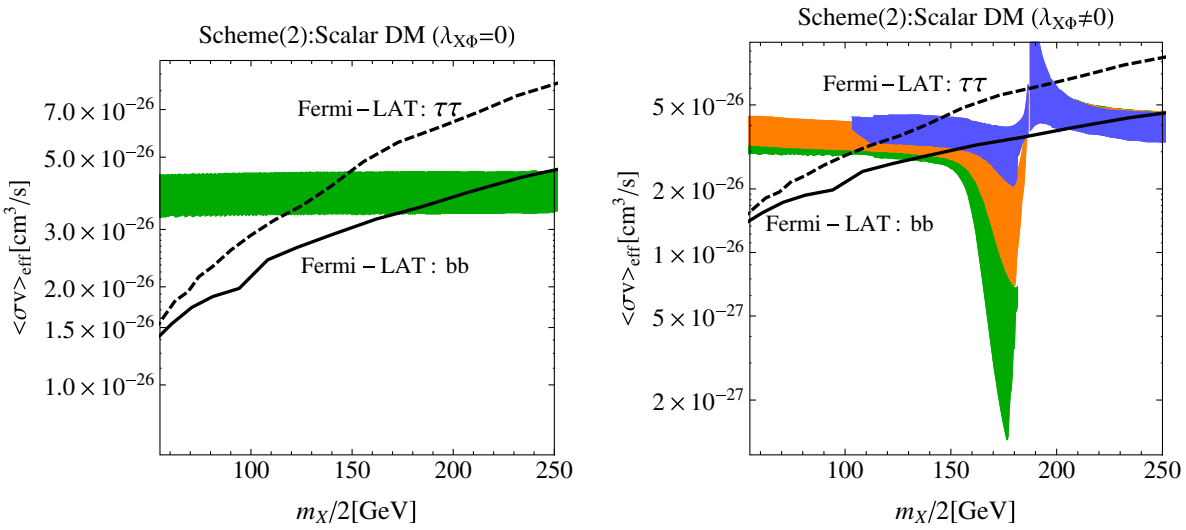

FIG. 7. The present-day effective thermally averaged cross section for $\langle\sigma v\rangle_{\rm eff}$ of Eq. (28) where the parameter region in Fig. 2 is applied. The black solid (dashed) line indicates the current limit of the cross section for the DMDM $\to b\bar{b}$ ($\tau\bar{\tau}$) annihilation mode from Fermi-LAT.

thermally averaged annihilation cross section for fermion DM is much smaller than the constraint by Fermi-LAT, and we omit the plots for this case.

IV. CONSTRAINTS FROM THE DIPHOTON RESONANCE SEARCH AND IMPLICATIONS FOR COLLIDER PHYSICS

In this section we discuss the constraints from current diphoton resonance data and search for the parameter region that is consistent with both the diphoton data and DM physics. Then, we shall consider the collider signatures in terms of the ϕ production cross section in that parameter region.

A. The constraint from the diphoton resonance search

Here we discuss the constraints from the diphoton resonance search in the model and search for the parameter region that is consistent with constraints from DM physics. In our scenario, the scalar boson ϕ provides a diphoton resonance where the mass of ϕ is set to 750 GeV as we mentioned above. ϕ can be produced by the gluon-fusion process through the effective interaction (17) at the LHC. The decay mode of $\phi \to \gamma\gamma$ is induced by the new fermion loop in the same way as the $\phi \to gg$. Then, we obtain the decay width of the diphoton mode as Eq. (A2). In the narrow-width approximation, the cross section for the process $pp \to \phi \to \gamma\gamma$ through gluon fusion can be expressed as [6]

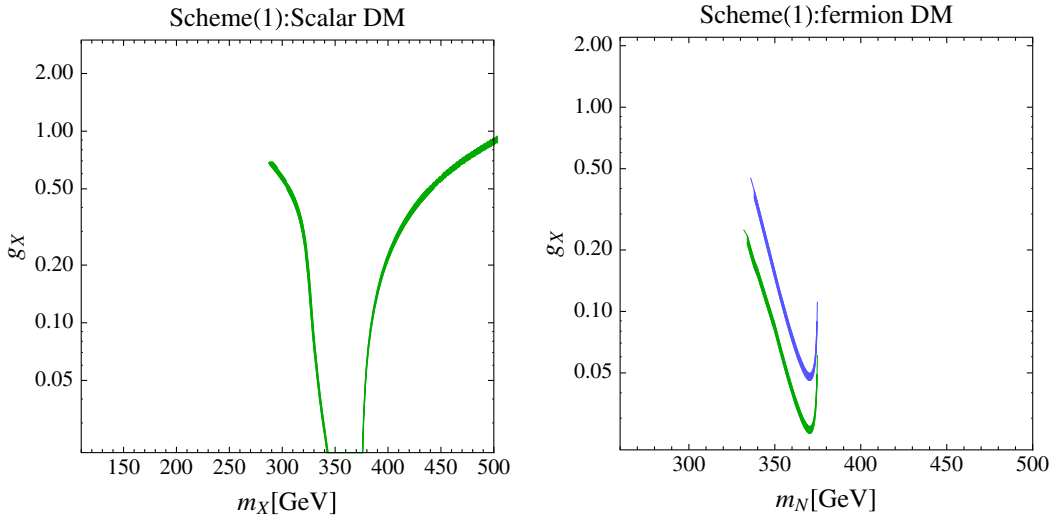

FIG. 8. The parameter region that can accommodate the relic density of DM and constraints from collider experiments for scalar and fermion DM in scheme 1).

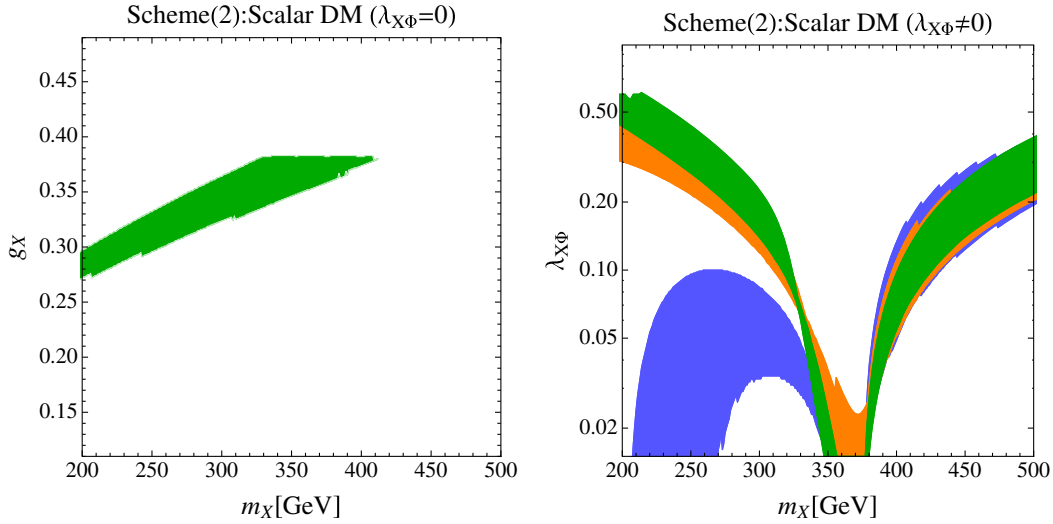

FIG. 9. The parameter region that can accommodate the thermal relic density of DM and constraints from collider experiments for scalar DM in scheme 2).

$$\sigma(pp \to \phi \to \gamma\gamma) \simeq \frac{C_{gg}}{s}\frac{\Gamma_{\phi\to gg}}{m_\phi}\mathrm{BR}(\phi \to \gamma\gamma), \quad (29)$$

where C_{gg} is related to the gluon luminosity function, s is the center of energy, and $\mathrm{BR}(\phi \to \gamma\gamma)$ is the branching fraction of $\phi \to \gamma\gamma$ decay. For $\sqrt{s} = 13(8)$ TeV, we adopt $C_{gg} \simeq 2137(174)$. In addition, we apply the K-factor for the gluon-fusion process as $K_{gg} \simeq 1.5$ [6]. Here we search for the parameter region that is allowed by the current diphoton resonance data and consistent with constraints from DM physics. We then estimate $\sigma(gg \to \phi \to \gamma\gamma)$, applying the parameter space that is consistent with constraints from DM physics for both schemes 1) and 2) in order to search for the region that is allowed by the current constraints from the diphoton resonance search. To satisfy the constraint, we require the cross section to be

$$\sigma(gg \to \phi \to \gamma\gamma) \leq 1.21 \text{ fb}, \quad (30)$$

where we take into account the 1σ error from the ATLAS result in Ref. [33]. We also apply constraints on the cross section for $pp \to \phi \to$ invisible from the monojet search data at the 8 TeV LHC [64]:

$$\sigma(pp \to \phi \to \text{invisible}) < 0.8 \text{ pb}. \quad (31)$$

We note that the process $pp \to \phi \to gg$ provides a dijet final state, but the cross sections in our model are smaller than the constraint from current dijet searches at a center of energy of $\sqrt{s} = 8$ or 13 TeV [65–67]. Here we comment on the case where ϕ is rather heavy, e.g., $m_\phi = 1.0$ and 1.5 TeV. In these cases, the ϕ production cross section becomes $\sigma_{m_\phi=1.0(1.5)\text{ TeV}} \simeq 0.42(0.19) \times \sigma_{m_\phi=750\text{ GeV}}$ when the other parameters have the same values as before. On the other hand, the current upper limit for $\sigma(gg \to \phi \to \gamma\gamma)$ from ATLAS is 0.78(0.48) fb for $m_\phi = 1.0(1.5)$ TeV. Therefore, the constraints from the diphoton mode are weaker for heavier m_ϕ since the production cross section rapidly decreases compared with the change in the upper limit.

In scheme 1), we obtain the allowed regions shown in Fig. 8 for the scalar and fermionic DM cases, which are consistent with the diphoton constraint and DM physics. We find that the region $m_X \lesssim 300$ GeV is excluded by Eq. (31) for the scalar DM case. Moreover, most of the parameter region is excluded by the diphoton constraint except for the region of 330 GeV $\lesssim m_N \lesssim$ 380 GeV for the

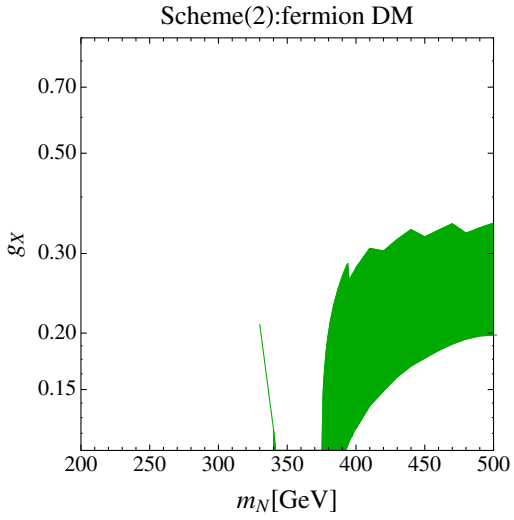

FIG. 10. The parameter region that can accommodate the relic density of DM and constraints from collider experiments for fermion DM in scheme 2).

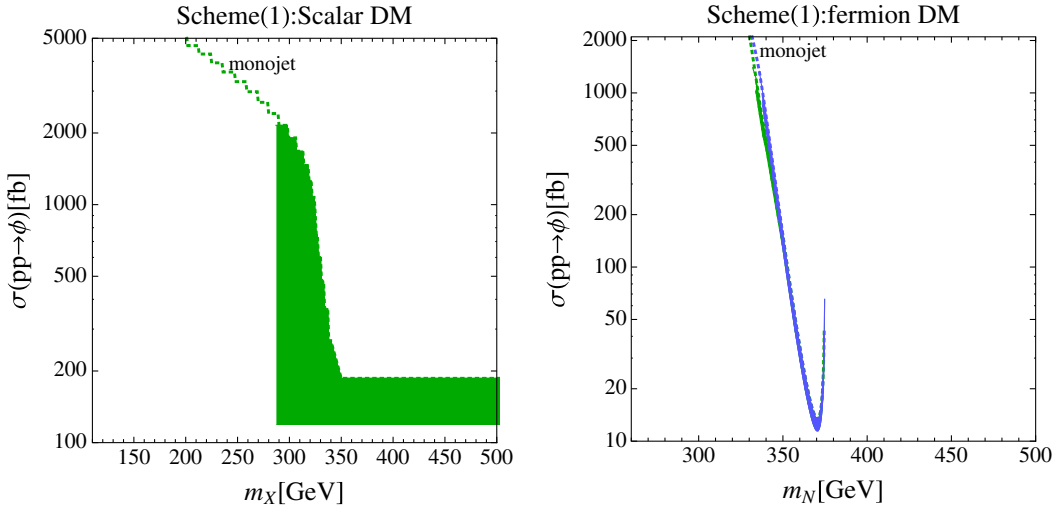

FIG. 11. The ϕ production cross section for the parameter region in Fig. 8. The dotted lines indicate the upper limits on the cross section from the $pp \to \phi \to XX$ channel with monojet search data at the LHC [64].

fermionic DM case. We note that in this scheme the width of ϕ is narrower than 1 GeV since ϕ decays via loop effects.

In scheme 2), we obtain the allowed regions in Figs. 9 and 10 for the scalar and fermion DM cases, respectively. For the scalar DM case with $\lambda_{X\Phi} = 0$, the region of $m_X \gtrsim 420$ GeV is excluded by the diphoton constraint. For the scalar DM case with $\lambda_{X\Phi} \neq 0$, we find that the DM mass region 200 GeV $\geq m_X \geq$ 500 GeV can accommodate the constraints (30) and (31). For the fermion DM case, we find that the region $m_X \lesssim 340$ GeV is excluded by Eq. (31). We note that in this scheme the width of ϕ is $O(10)$ to $O(50)$ GeV for $m_\phi > 2m_{Z'}$ and less than 1 GeV for $m_\phi < 2m_{Z'}$.

B. The ϕ production cross section

Here we explore the ϕ production cross section for the parameter region that is consistent with the constraints from collider experiments and DM physics. The ϕ production cross section is derived from Eq. (29). For scheme 1), we show the cross sections in Fig. 11 which are obtained by applying the parameter space shown in Fig. 8. We then have a $O(100)$ $(O(10))$ to $O(1000)$ fb cross section for the scalar (fermion) DM case for the allowed region. Since ϕ mainly decays into two gluons in scheme 1), the dijet event is another signature of ϕ as $pp \to \phi \to jj$, which can be tested at the LHC.

For scheme 2), we obtain the cross sections shown in Figs. 12 and 13 which are obtained by applying the

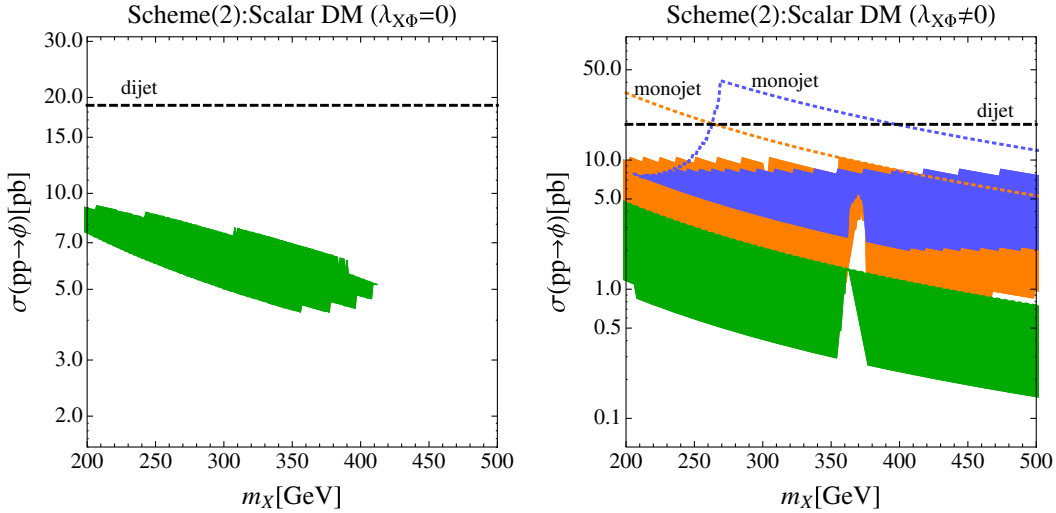

FIG. 12. The ϕ production cross section for the parameter region in Fig. 9. The dashed line indicates the upper limit on the cross section from the dijet search at the LHC [65] for BR$(\phi \to jj) = 1.0$. The dotted lines in the right panel are the monojet constraints as in Fig. 11.

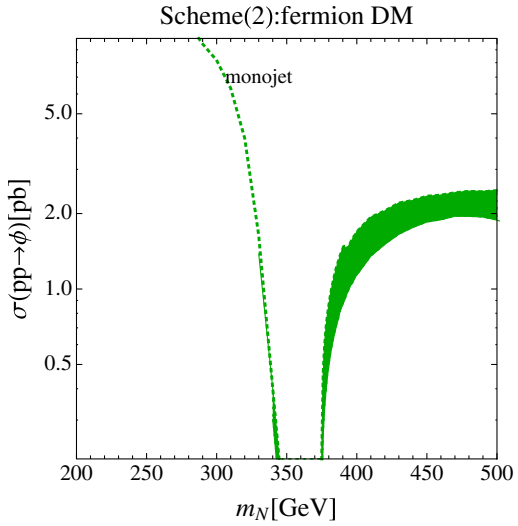

FIG. 13. The ϕ production cross section for the parameter region in Fig. 10. The dotted line indicates the monojet constraints as in Figs. 11 and 12.

parameter spaces in Figs. 9 and 10, respectively. We then find that a ∼4 to ∼9 pb cross section is obtained for the allowed region for $\lambda_{X\Phi} = 0$, while a ∼0.2 to ∼10 pb cross section is obtained for $\lambda_{X\Phi} \neq 0$. These cross sections are constrained when the $\phi \to Z'Z'$ mode is kinematically allowed, since Z' can decay into SM leptons with $\mathrm{BR}(\phi \to \ell^+\ell^-) \sim O(20)\%$ via kinetic mixing [5], which induces signal events such as $2j + ll$, $4l$, and $2l + \not{E}_T$. We also have the signal events $4j$ and $2j + \not{E}_T$, but they will be less significant due to large SM backgrounds. A detailed analysis of current experimental constraints for the $pp \to \phi \to Z'Z'$ process is beyond the scope of this paper and we leave it for future work. We also would like to comment that the branching fraction of Z' would be modified with a nonzero Yukawa coupling $Ff_{\mathrm{SM}}X$ at loop level since the kinetic mixing is very small.

V. SUMMARY AND DISCUSSION

In this paper, we have investigated dark matter physics for the chiral dark sector model where dark fermions are vector-like under $\mathrm{SU}(3) \times \mathrm{U}(1)_Y$ but chiral under dark $\mathrm{U}(1)_X$ gauge symmetry. In our model, the extra scalar bosons with nonzero $\mathrm{U}(1)_X$ (Φ and X in Table I) are also introduced in order to break the U(1) symmetry spontaneously and to make dark fermions decay, respectively. As a result of our setup, we have accidental Z_2 symmetry which guarantees the stability of our DM candidate: a scalar boson X and a neutral dark fermion N. We also have a massive new gauge boson Z' after spontaneous breaking of $\mathrm{U}(1)_X$ gauge symmetry.

In our analysis of DM physics, two different schemes were considered: 1) $m_{\mathrm{DM}} < m_{Z'}$ and 2) $m_{\mathrm{DM}} > m_{Z'}$, where m_{DM} and $m_{Z'}$ are the DM mass and mass of the Z' boson, respectively. For scheme 1), the dominant DM annihilation process is DMDM → gg [exchanging the scalar boson ϕ associated with $\mathrm{U}(1)_X$ breaking], while the dominant annihilation process for scheme 2) is DMDM → $Z'Z'$. Then, we investigated the relic density of DM, the DM-nucleon scattering cross section for direct detection, and the DM annihilation cross section for indirect detection to find the parameter region that is allowed by constraints from current observations. In our analysis we fixed the dark fermion masses to reduce the number of free parameters, and explored the parameter space of DM masses, the Z' mass, g_X, and the coupling constant $\lambda_{X\Phi}$ for the $\Phi\Phi XX$ interaction in both schemes.

For scheme 1), the relic density of DM is determined by the annihilation cross section for $XX(NN) \to gg$ processes. Then, we showed the allowed parameter space providing the observed relic density in the m_X-$\lambda_{X\Phi}$ and m_N-g_X planes for the scalar and fermion DM cases, respectively. We found that the $m_X \gtrsim 140$ GeV region can provide the observed relic density with $\lambda_{X\Phi} < \sqrt{4\pi}$ for scalar DM, while fermion DM can have the right relic density in all DM mass regions that we considered. These parameter regions are further constrained by direct and indirect detection experiments. The parameter region with $m_X \lesssim 200$ GeV is excluded for scalar DM, whereas the $m_N \lesssim 300$ GeV region is excluded for fermion DM when $m_{Z'} = 1.1 m_N$. On the other hand, constraints from indirect detection exclude the region with $m_X \simeq m_\phi/2$ for scalar DM, whereas no further constraint is imposed for fermion DM.

For scheme 2), the thermal relic density is determined by the annihilation cross section for $XX(NN) \to Z'Z'$ processes. The allowed parameter regions that give the right relic density for scalar DM were shown in the m_X-g_X (with $\lambda_{X\Phi} = 0$) and m_X-$\lambda_{X\Phi}$ planes (with several values of g_X), while the allowed parameter region for fermion DM was shown in the m_N-g_X plane. Then, we showed that the current constraints from direct detection exclude some regions with $m_X \lesssim 150$ GeV and $g_X = 0.1$ for scalar DM, and the DM-nucleon scattering cross section is below the current limit for fermion DM. We also found that the parameter region with $m_X \lesssim 200$ GeV is constrained by the Fermi-LAT data for scalar DM, while fermion DM is free from indirect detection constraints due to the absence of a s-channel annihilation mode. The parameter spaces can be further tested in future direct and indirect detection experiments for both schemes.

Finally, we also investigated constraints from collider experiments including the diphoton resonance search by ATLAS and CMS at the 13 TeV LHC and searched for the parameter region which can accommodate both DM and collider constraints. In our model a source of diphoton resonance is the scalar boson ϕ, which is nothing but a remnant of $\mathrm{U}(1)_X$ breaking by the dark Higgs mechanism. The cross section for $pp \to \phi \to \gamma\gamma$ was estimated by applying parameter sets that can provide the correct thermal

relic density of DM. Then, we showed the parameter regions that can accommodate the constraint from the diphoton resonance search for both schemes with scalar and fermion DM. In addition, we have discussed the ϕ production cross section and applied the appropriate parameter regions. We found that the cross section in scheme 2) tends to be larger than that in scheme 1). The signatures of ϕ other than the diphoton event are dijet and $Z'Z'$ events for scheme 1) and scheme 2), respectively, where Z' decays into a SM fermion pair, thereby providing four SM fermion final states. A detailed analysis of signals and backgrounds is beyond the scope of this paper and we leave it for future work.

Before closing, we comment on the stability of the potential in our model. In the previous study [5], we discussed the stability of the scalar potential within the renormalization group running and found that our model could be valid up to $\sim O(10)$ TeV with $O(1)$ Yukawa couplings and other couplings in the scalar potential. In the present analysis, we were able to take smaller couplings since the cross section for $pp \to \phi \to \gamma\gamma$ should be smaller than our previous analysis, and thus the stability could be achieved up to a higher scale.

ACKNOWLEDGMENTS

This work is supported in part by the National Research Foundation of Korea (NRF) Research Grant No. NRF-2015R1A2A1A05001869, and by the NRF grant funded by the Korea government (MSIP) (No. 2009-0083526) through the Korea Neutrino Research Center at Seoul National University (PK).

APPENDIX: THE DECAY WIDTHS OF ϕ

Here we summarize the decay widths of ϕ which are given in Ref. [5]. The width for the $\phi \to gg$ mode is given by

$$\Gamma_{\phi\to gg} = \frac{\alpha_s^2 m_\phi^3}{32\pi^3}\left|\sum\nolimits_{F=U,D}\frac{(a+b)g_X}{2m_{Z'}}A_{1/2}(\tau_F)\right|^2. \quad \text{(A1)}$$

Similarly, the partial decay width for $\phi \to \gamma\gamma$ is given by

$$\Gamma_{\phi\to\gamma\gamma} = \frac{\alpha^2 m_\phi^3}{256\pi^3}\left|\sum\nolimits_{F}N_c^F\frac{(a+b)g_X Q_F^2}{m_{Z'}}A_{1/2}(\tau_F)\right|^2, \quad \text{(A2)}$$

where Q_F and N_c^F are the electric charge and number of colors of exotic fermions F. The formula for the partial decay width of $\phi \to Z\gamma$ is

$$\begin{aligned}\Gamma_{\phi\to Z\gamma} &= \frac{m_\phi^3}{32\pi}|A_{Z\gamma}|^2\left(1-\frac{m_Z^2}{m_\phi^2}\right)^3,\\ A_{Z\gamma} &= \frac{2\sqrt{2}\alpha s_W g_X}{\pi c_W}\sum_F\frac{N_c^F(a+b)Q_F^2}{m_{Z'}}[I_1(\tau_F,\lambda_F)\\ &\quad - I_2(\tau_F,\lambda_F)],\end{aligned} \quad \text{(A3)}$$

where $\lambda_F = 4m_F^2/m_Z^2$ and the corresponding loop integrals are given by [53]

$$\begin{aligned}I_1(x,y) &= \frac{xy}{2(x-y)}+\frac{x^2y^2}{2(x-y)^2}[f(x)^2-f(y)^2]\\ &\quad +\frac{x^2 b}{(x-y)^2}[g(x)-g(y)],\\ I_2(x,y) &= -\frac{xy}{2(x-y)}[f(x)^2-f(y)^2],\\ g(t) &= \sqrt{t-1}\sin^{-1}(1/\sqrt{t}).\end{aligned} \quad \text{(A4)}$$

The decay widths of ϕ into $Z'Z'$, X^*X, and $\bar{F}F$ modes are obtained at tree level as

$$\begin{aligned}\Gamma_{\phi\to Z'Z'} &= \frac{(a+b)^2 g_X^2 m_{Z'}^2}{32\pi m_\phi}\frac{m_\phi^4-4m_\phi^2 m_{Z'}^2+12m_{Z'}^4}{m_{Z'}^4}\\ &\quad\times\sqrt{1-\frac{4m_{Z'}^2}{m_\phi^2}},\end{aligned} \quad \text{(A5)}$$

$$\Gamma_{\phi\to X^*X} = \frac{\lambda_{X\Phi}^2 m_{Z'}^2}{16\pi(a+b)^2 g_X^2 m_\phi}\sqrt{1-\frac{4m_X^2}{m_\phi^2}}, \quad \text{(A6)}$$

$$\Gamma_{\phi\to\bar{F}F} = \frac{g_X^2 M_F^2}{4\pi m_{Z'}^2}m_\phi\sqrt{1-\frac{4M_F^2}{m_{Z'}^2}}. \quad \text{(A7)}$$

[1] M. Aaboud *et al.* (ATLAS Collaboration), J. High Energy Phys. 09 (2016) 001.
[2] V. Khachatryan *et al.* (CMS Collaboration), Phys. Rev. Lett. **117**, 051802 (2016).
[3] ATLAS Collaboration, Report No. ATLAS-CONF-2016-018.
[4] CMS Collaboration, Report No. CMS-PAS-EXO-16-018.
[5] P. Ko and T. Nomura, Phys. Lett. B **758**, 205 (2016).

[6] R. Franceschini, G. F. Giudice, J. F. Kamenik, M. McCullough, A. Pomarol, R. Rattazzi, M. Redi, F. Riva, A. Strumia, and R. Torre , J. High Energy Phys. 03 (2016) 144.
[7] K. Harigaya and Y. Nomura, Phys. Lett. B **754**, 151 (2016).
[8] M. Backovic, A. Mariotti, and D. Redigolo, J. High Energy Phys. 03 (2016) 157.
[9] A. Angelescu, A. Djouadi, and G. Moreau, Phys. Lett. B **756**, 126 (2016).
[10] Y. Nakai, R. Sato, and K. Tobioka, Phys. Rev. Lett. **116**, 151802 (2016).
[11] D. Buttazzo, A. Greljo, and D. Marzocca, Eur. Phys. J. C **76**, 116 (2016).
[12] S. Di Chiara, L. Marzola, and M. Raidal, Phys. Rev. D **93**, 095018 (2016).
[13] S. Knapen, T. Melia, M. Papucci, and K. Zurek, Phys. Rev. D **93**, 075020 (2016).
[14] A. Pilaftsis, Phys. Rev. D **93**, 015017 (2016).
[15] J. Ellis, S. A. R. Ellis, J. Quevillon, V. Sanz, and T. You, J. High Energy Phys. 03 (2016) 176.
[16] R. S. Gupta, S. Jager, Y. Kats, G. Perez, and E. Stamou, J. High Energy Phys. 07 (2016) 145.
[17] A. Kobakhidze, F. Wang, L. Wu, J. M. Yang, and M. Zhang, Phys. Lett. B **757**, 92 (2016).
[18] A. Falkowski, O. Slone, and T. Volansky, J. High Energy Phys. 02 (2016) 152.
[19] R. Benbrik, C. H. Chen, and T. Nomura, Phys. Rev. D **93**, 055034 (2016).
[20] R. Ding, L. Huang, T. Li, and B. Zhu, arXiv:1512.06560.
[21] F. Wang, L. Wu, J. M. Yang, and M. Zhang, Phys. Lett. B **759**, 191 (2016).
[22] P. S. B. Dev and D. Teresi, Phys. Rev. D **94**, 025001 (2016).
[23] B. C. Allanach, P. S. B. Dev, S. A. Renner, and K. Sakurai, Phys. Rev. D **93**, 115022 (2016).
[24] K. Cheung, P. Ko, J. S. Lee, J. Park, and P. Y. Tseng, Phys. Rev. D **94**, 033010 (2016).
[25] F. Wang, W. Wang, L. Wu, J. M. Yang, and M. Zhang, arXiv:1512.08434.
[26] C. W. Chiang, M. Ibe, and T. T. Yanagida, J. High Energy Phys. 05 (2016) 084.
[27] X. J. Huang, W. H. Zhang, and Y. F. Zhou, Phys. Rev. D **93**, 115006 (2016).
[28] S. Kanemura, K. Nishiwaki, H. Okada, Y. Orikasa, S. C. Park, and R. Watanabe, arXiv:1512.09048.
[29] T. Nomura and H. Okada, Phys. Lett. B **755**, 306 (2016).
[30] P. Ko, Y. Omura, and C. Yu, J. High Energy Phys. 04 (2016) 098.
[31] T. Nomura and H. Okada, arXiv:1601.04516.
[32] CMS Collaboration, Report No. CMS-PAS-EXO-16-027.
[33] ATLAS Collaboration, Report No. ATLAS-CONF-2016-059.
[34] S. Baek, P. Ko, and W. I. Park, J. High Energy Phys. 07 (2013) 013.
[35] C. W. Chiang, T. Nomura, and J. Tandean, J. High Energy Phys. 01 (2014) 183.
[36] E. Dudas, L. Heurtier, Y. Mambrini, and B. Zaldivar, J. High Energy Phys. 11 (2013) 083.
[37] A. Alves, S. Profumo, and F. S. Queiroz, J. High Energy Phys. 04 (2014) 063.
[38] P. Ko and Y. Tang, J. Cosmol. Astropart. Phys. 05 (2014) 047.
[39] P. Ko and Y. Tang, J. Cosmol. Astropart. Phys. 01 (2015) 023.
[40] S. Baek, P. Ko, and W. I. Park, Phys. Lett. B **747**, 255 (2015).
[41] R. Martinez, J. Nisperuza, F. Ochoa, and J. P. Rubio, Phys. Rev. D **90**, 095004 (2014).
[42] R. Martinez, J. Nisperuza, F. Ochoa, J. P. Rubio, and C. F. Sierra, Phys. Rev. D **92**, 035016 (2015).
[43] A. Alves, A. Berlin, S. Profumo, and F. S. Queiroz, Phys. Rev. D **92**, 083004 (2015).
[44] J. Guo, Z. Kang, P. Ko, and Y. Orikasa, Phys. Rev. D **91**, 115017 (2015).
[45] A. Alves, A. Berlin, S. Profumo, and F. S. Queiroz, J. High Energy Phys. 10 (2015) 076.
[46] O. Ducu, L. Heurtier, and J. Maurer, J. High Energy Phys. 03 (2016) 006.
[47] R. Martinez and F. Ochoa, J. High Energy Phys. 05 (2016) 113.
[48] S. Choi, S. Jung, and P. Ko, J. High Energy Phys. 10 (2013) 225.
[49] K. Cheung, P. Ko, J. S. Lee, and P. Y. Tseng, J. High Energy Phys. 10 (2015) 057.
[50] A. Hook, E. Izaguirre, and J. G. Wacker, Adv. High Energy Phys. **2011**, 859762 (2011).
[51] S. Andreas, C. Niebuhr, and A. Ringwald, Phys. Rev. D **86**, 095019 (2012).
[52] J. Jaeckel, M. Jankowiak, and M. Spannowsky, Phys. Dark Univ. **2**, 111 (2013).
[53] J. F. Gunion, H. E. Haber, G. L. Kane, and S. Dawson, Front. Phys. **80**, 1 (2000).
[54] A. Ibarra, T. Toma, M. Totzauer, and S. Wild, Phys. Rev. D **90**, 043526 (2014).
[55] F. Giacchino, A. Ibarra, L. L. Honorez, M. H. G. Tytgat, and S. Wild, J. Cosmol. Astropart. Phys. 02 (2016) 002.
[56] P. Gondolo and G. Gelmini, Nucl. Phys. **B360**, 145 (1991).
[57] G. Belanger, F. Boudjema, A. Pukhov, and A. Semenov, Comput. Phys. Commun. **192**, 322 (2015).
[58] P. A. R. Ade *et al.* (Planck Collaboration), Astron. Astrophys. **571**, A16 (2014).
[59] J. Hisano, R. Nagai, and N. Nagata, J. High Energy Phys. 05 (2015) 037.
[60] D. S. Akerib *et al.* (LUX Collaboration), Phys. Rev. Lett. **112**, 091303 (2014).
[61] D. S. Akerib *et al.* (LUX Collaboration), Phys. Rev. Lett. **116**, 161301 (2016).
[62] E. Aprile *et al.* (XENON Collaboration), J. Cosmol. Astropart. Phys. 04 (2016) 027.
[63] M. Ackermann *et al.* (Fermi-LAT Collaboration), Phys. Rev. Lett. **115**, 231301 (2015).
[64] V. Khachatryan *et al.* (CMS Collaboration), Eur. Phys. J. C **75**, 235 (2015).
[65] G. Aad *et al.* (ATLAS Collaboration), Phys. Rev. D **91**, 052007 (2015).
[66] V. Khachatryan *et al.* (CMS Collaboration), Phys. Rev. Lett. **116**, 071801 (2016).
[67] G. Aad *et al.* (ATLAS Collaboration), Phys. Lett. B **754**, 302 (2016).